Design considerations for open-well microfluidic platforms for hypoxic cell studies

Cite as: Biomicrofluidics **11**, 054116 (2017); https://doi.org/10.1063/1.4998579
Submitted: 01 August 2017 • Accepted: 03 October 2017 • Published Online: 27 October 2017

Matthew B. Byrne, Matthew T. Leslie, Heeral S. Patel, et al.

Design considerations for open-well microfluidic platforms for hypoxic cell studies

Matthew B. Byrne,[1,2,a)] Matthew T. Leslie,[2,4,5,a)] Heeral S. Patel,[1] H. Rex Gaskins,[2,3,4,5] and Paul J. A. Kenis[1,2,5,b)]
[1]*Department of Chemical and Biomolecular Engineering, University of Illinois at Urbana-Champaign, Urbana, Illinois 61801, USA*
[2]*Carl R. Woese Institute for Genomic Biology, University of Illinois at Urbana-Champaign, Urbana, Illinois 61801, USA*
[3]*Department of Animal Sciences, University of Illinois at Urbana-Champaign, Urbana, Illinois 61801, USA*
[4]*Department of Pathobiology, University of Illinois at Urbana-Champaign, Urbana, Illinois 61801, USA*
[5]*Midwest Cancer Nanotechnology Training Center, University of Illinois at Urbana-Champaign, Urbana, Illinois 61801, USA*

(Received 1 August 2017; accepted 3 October 2017; published online 27 October 2017)

Regions of hypoxia are common in solid tumors and are associated with enhanced malignancy, metastasis, and chemo/radio resistance. Real-time hypoxic cellular experimentation is challenging due to the constant need for oxygen control. Most microfluidic platforms developed thus far for hypoxic cell studies are burdened by complex design parameters and are difficult to use for uninitiated investigators. However, open-well microfluidic platforms enable short and long term hypoxic cell studies with an ease of use workflow. Specifically, open-well platforms enable manipulation and addition of cells, media, and reagents using a micropipette for hypoxic cell studies in tunable dissolved oxygen concentrations as low 0.3 mg/l. We analyzed design considerations for open-well microfluidic platforms such as media height, membrane thickness, and impermeable barriers to determine their effects on the amount of dissolved oxygen within the platform. The oxygen concentration was determined by experimental measurements and computational simulations. To examine cell behavior under controlled oxygen conditions, hypoxia-induced changes to hypoxia inducible factor activity and the mitochondrial redox environment were studied. A fluorescent reporter construct was used to monitor the stabilization of hypoxia inducible factors 1α and 2α throughout chronic hypoxia. Reporter construct fluorescence intensity inversely correlated with dissolved oxygen in the medium, as expected. Additionally, the glutathione redox poise of the mitochondrial matrix in living cancer cells was monitored throughout acute hypoxia with a genetically encoded redox probe and was observed to undergo a reductive response to hypoxia. Overall, these studies validate an easy to use open-well platform suitable for studying complex cell behaviors in hypoxia. *Published by AIP Publishing*. https://doi.org/10.1063/1.4998579

I. INTRODUCTION

In solid tumors, poorly arranged and malfunctioning vasculature can cause regions that exhibit physiologically low levels of oxygen.[1–5] These hypoxic regions present a unique set of challenges in the treatment of solid tumors. Clinically, tumor hypoxia is a negative prognostic indicator for a more aggressive phenotype and is associated with the therapeutic resistance.[6,7] Functional definitions of hypoxia often differ among disciplines, and, as a result, widely varying

[a)]M. B. Byrne and M. T. Leslie contributed equally to this work.
[b)]Author to whom correspondence should be addressed: kenis@illinois.edu. Telephone: (217)244-9214. Fax: (217)333-5052.

"hypoxic" oxygen levels are reported in the literature.[3,8] Furthermore, *in vivo* measures of tumoral hypoxia also range broadly depending on the tissue of origin, cancer subtype, disease stage, the presence of other complicating medical factors, and the method of oxygen measurement.[8] Table I displays oxygenation values for a number of malignancies compared to respective "normal" tissues.[2]

One defining cellular response to hypoxia is the stabilization of the alpha subunit of the heterodimeric transcription factor hypoxia inducible factor (HIF). In the presence of physiologic oxygen, HIF-1α and HIF-2α (herein referred to collectively as HIF-α) are constitutively expressed, marked for ubiquitination via oxygen-sensitive prolyl hydroxylases, and subsequently degraded.[9–11] However, in low oxygen environments, this process is interrupted, whereby the alpha subunits accumulate and dimerize with a HIF-β subunit, generating a functional HIF heterodimer.[11] The HIF heterodimer serves as a major transcription factor, inducing the expression of more than 100 genes, including those that regulate metabolism, cell signaling, erythropoiesis, angiogenesis, cell proliferation, and apoptosis.[12] Another defining cellular response to hypoxia is mitochondrial generation of reactive oxygen species (ROS). The enhanced production of mitochondrial-derived ROS in hypoxia has been hypothesized to represent a cellular response to lowered oxygen availability and is necessary for the stabilization of HIF.[13–15] Studies using live cell glutathione redox biosensors to indirectly monitor ROS production in hypoxia, combined with pharmacologic and genetic modulation of antioxidant systems, have provided a well-characterized map of subcellular responses to lowered oxygen tensions.[16–24] During hypoxia, ROS are produced on the outer leaflet of the inner mitochondrial membrane, which oxidizes the mitochondrial intermembrane space and cytosol and stabilizes HIF-α.[14,20] Furthermore, hypoxic ROS production is accompanied by reduction of glutathione in the mitochondrial matrix, perhaps because ROS usually generated in the mitochondrial matrix are directed outward into the intermembrane space and cytosol during hypoxia.[20,22,23] Thus, hypoxia induces differential subcellular redox responses that may regulate cellular signaling, as well as metabolic responses to lowered oxygen tensions. Given this, it is important to match *in vitro* studies as closely as possible to the *in vivo* conditions of the tumor microenvironment. However, even simple *in vitro* hypoxic studies are complicated by the rigors of hypoxic experimentation and the need for constant oxygen control. Therefore, methods that enable control over oxygen conditions during cell studies are essential to understand the behavior of cancer cells under hypoxia.

Microfluidic platforms have been developed to control oxygen concentrations within the cellular microenvironment.[25] One approach is to fabricate platforms from gas impermeable materials to create closed systems with controlled oxygenation values.[26–30] In contrast, other devices fabricated with gas permeable materials have cell chambers located adjacent to and equilibrated with hypoxic gas channels.[31–36] In general, these devices enable real-time imaging of cellular events and reduce equilibration times compared to conventional hypoxic study

TABLE I. Oxygenation values of interest in hypoxic tumor cell biology. Values are presented in partial pressure of oxygen (mm Hg) and concentration of oxygen (mg/l). Oxygenation values are medians of individual values that were measured in mm Hg using an oxygen electrode. All pO_2 and cO_2 data are obtained from the study by Brown and Wilson.[2]

	Median diseased		Median healthy	
Tumor type	pO_2 (mmHg)	cO_2 (mg/l)	pO_2 (mmHg)	cO_2 (mg/l)
Breast cancer	10	0.58	…	…
Cervical cancer	3.0–5.0	0.18–0.29	51	3.0
Glioblastoma	4.9–5.6	0.29–0.33	…	…
Head and neck carcinoma	12.2–14.7	0.71–0.86	40–51.2	2.3–3.0
Lung cancer	7.5	0.44	38.5	2.2
Pancreatic cancer	2.7	0.16	51.6	3.0
Prostate cancer	2.4	0.14	30	1.7
Soft-tissue sarcoma	6.2–18	0.36–1.0	…	…

methods such as gas-controlled incubators.[32,37] Still, a limitation of many of the platforms developed to date is their difficult fabrication and experimental use. Accordingly, microfluidic platforms with chambers that are open to the atmosphere have been developed.[38–40] These devices enable easy manipulation of cells, media, and reagents using a micropipette while still controlling oxygen tensions. However, the design considerations that affect oxygen conditions within these microfluidic platforms have not been fully characterized.

Here, we present the effects of design considerations on the oxygen concentration within an open-well microfluidic platform for cell studies. The platform enables control of dissolved oxygen ranging from 6.5 mg/l to 0.3 mg/l, an ideal range for the study of hypoxia in tumor microenvironments.[2] The open-well design allows for cells and reagents to be added using a micropipette, thus eliminating the need for ancillary pumps and tubing common in microfluidic culture systems. The amount of dissolved oxygen within the platform was experimentally and computationally determined with varying platform parameters such as gas composition, addition of a gas-impermeable barrier, membrane thickness, and media height. Arguably, the two most physiologically important aspects of cellular hypoxia are the stabilization of the major transcription factor HIF and the mitochondrial production of reactive oxygen species. Therefore, Chinese hamster ovary (CHO) cells expressing an HIF reporter construct were introduced within the platform and exposed to chronic hypoxia. HIF activity levels at varying amounts of dissolved oxygen were monitored via eYFP fluorescence. Furthermore, A549 lung adenocarcinoma cells expressing the Grx1-roGFP2 redox biosensor were cultured within the platform, and the redox state of the mitochondrial matrix during acute hypoxia was examined. These studies fully characterize a microfluidic platform in which complex hypoxic cell studies can be conducted by researchers with minimal microfluidic expertise.

II. EXPERIMENTAL MATERIALS AND METHODS

A. Platform fabrication and design

To create the gas channel layer, high-resolution printing (5080 dpi) was used to create a mask with the designed pattern on a transparency film. The mask was used to pattern 20 μm high features out of SU-8 2025 photoresist (Microchem, Newton, MA) on a silicon wafer by photolithography.[41–43] Poly(dimethysiloxane) (PDMS; General Electric RTV 650 Part A/B, Niskayuna, NY) was patterned on the silicon wafer by spin-coating and curing the pre-polymer for 30 min at 70 °C.[44] The cell chamber was created by punching a 4-mm wide hole in a cured PDMS slab. The PDMS slab was then irreversibly bonded to the gas layer by treatment with air plasma for 90 s (Model PDC-001, Harrick Scientific, Pleasantville, NY). Inlets and outlets for the gas stream were created in PDMS using a 23 G steel punch. The surface of the PDMS replica and a clean glass coverslip (Fisher Scientific, Waltham, MA) were treated with air plasma for 90 s and irreversibly bonded to complete the device assembly. The device inlets were then connected to a gas cylinder (SJ Smith, Urbana, IL) with PTFE tubing (24 G, Cole-Parmer, Vernon Hills, IL), and the gas flow rate was controlled via a mass flow controller (Sierra Instruments SmartTrak 2, Monterey, CA).

B. PDMS membrane thickness

The PDMS membrane thickness was controlled by spincoating PDMS at calibrated rotational speeds. To measure the membrane thickness, images of the membranes were acquired using an optical microscope (Leica Z16 APO) equipped with a digital camera (Leica DFC280). The membrane was imaged on its side in order to determine the thickness. The thickness of the membrane was then measured by analyzing the images using ImageJ (NIH).

C. Cell culture and genetic construct

Chinese hamster ovary (CHO) cells (ATCC CCL-61, Manassas, VA) were cultured in Dulbecco's modified eagle medium supplemented with 10% fetal bovine serum (FBS) (Gemini Bio-Products, Woodland, CA) and 100 U/ml penicillin/streptomycin (Gibco, Carlsbad, CA). Lung carcinoma A549 cells, a gift from Dr. Paul Hergenrother (University of Illinois), were cultured in

Roswell Park memorial institute medium 1640 supplemented with 10% fetal bovine serum (Gemini Bio-Products) and 100 U/ml penicillin/streptomycin (Gibco). All cells were cultured at 37 °C with 5% CO_2 and passaged regularly at 70%–80% confluence. All experiments were performed on sub-confluent cultures in Matrigel (BD Biosciences, San Jose, CA) within the microfluidic device. Cells were encapsulated in Matrigel by mixing at a volumetric ratio of 30 cells:70 Matrigel and were loaded into the device via a micropipette.

D. Stable expression of genetic constructs

Stable expression of the 6U-HBR plasmid (plasmid 42621, Addgene, Cambridge, MA) in CHO cells was achieved via lentiviral transduction.[45] To produce lentiviral particles, the 6 U-HBR plasmid was transfected into HEK293T cells (Invitrogen, Carlsbad, CA) by lipofectamine transfection (Life Technologies, Carlsbad, CA) as suggested by the manufacturer.[45] The medium was changed 24 h after transfection, and viral supernatants were collected and filtered after 72 h. The viral supernatants were centrifuged at 6000 rpm for 45 min at 4 °C. The concentrated viral particles were then added into the CHO cell medium, creating a stably transfected cell line. After creation of the stable cell line, cells were harvested and resuspended at a concentration of 10^6 cells/ml.

The mitochondrial matrix targeted redox-sensitive biosensor Grx1-roGFP2 was a gift from Dr. Tobias Dick (German Cancer Research Center, Heidelberg, Germany). The original construct was subcloned into a lentiviral pCDH-CMV-MCS-EF1-puro vector (System Biosciences, Palo Alto, CA). Plasmid transfection to generate viral particles was performed using Lipofectamine 2000 according to manufacturer protocols.

E. Chemicals and reagents

Diamide and DTT (Sigma Aldrich, St. Louis, MO) were resuspended in Dulbecco's phosphate buffered saline (Mediatech, Manassas, VA) and delivered sequentially via micropipette bolus addition following each experiment for redox calibration. A fluorescent dye, ruthenium tris(2,2′-dipyridyl) dichloride hexahydrate (RTDP) (Sigma Aldrich), was used to experimentally measure the amount of dissolved oxygen in solution in the microfluidic platform. An oxygen scavenging chemical, sodium sulfite (Sigma Aldrich), was used to calibrate the fluorescent dye by creating an anoxic state.

F. Experimental measurement of dissolved oxygen

To measure the amount of dissolved oxygen within the microfluidic platform, the RTDP fluorescent dye was introduced into the cell chamber of the platform.[46,47] The fluorescence of RTDP is quenched in the presence of oxygen. Thus, by starting at atmospheric conditions (9.1 mg/l O_2) and then introducing gas into the platform, the change in fluorescence intensity can be related to the amount of dissolved oxygen using the Stern-Volmer equation [Eq. (1)]:

$$\frac{I_0}{I} = 1 + K_q[O_2]. \tag{1}$$

The uninhibited dye intensity, I_0, was found by introducing sodium sulfite, an oxygen-scavenging chemical, to create anoxic (0.0 mg/l O_2) conditions and calibrate the readings.[48–50] Sodium sulfite has been demonstrated to create anoxic conditions in liquids exposed to the atmosphere.[50] The quenching constant, K_q, was calibrated using the fluorescence intensity at atmospheric and anoxic conditions. The images were acquired with the platform loaded onto a stage heated to 37 °C and using an inverted fluorescent microscope (Leica DMI 400b) with a 20×0.4 NA objective. The fluorescence intensity was measured using ImageJ ROI manager.[51,52]

G. Computational modeling of dissolved oxygen within the microfluidic platform

A computational model of the microfluidic platform was constructed using the finite element analysis software Comsol (Comsol, Burlington, MA). Transient and steady-state numerical simulations were performed by solving the convection-diffusion equation. The simulations

enabled investigation and computation of the amount of dissolved oxygen in the device when parameters such as PDMS membrane thickness, media height, and gas stream composition varied.

The amount of dissolved oxygen in solution is dependent upon the amount of salt and temperature in the solution. For experiments using the medium at 37 °C, the initial oxygen concentration is modeled to be 6.5 mg/l O_2. For experiments using water at room temperature, the starting oxygen concentration is modeled to be 9.0 mg/l O_2.

H. Microscopy and image processing of HIF-α stabilization experiments

Cells were incubated in the microfluidic platform in an incubator at 37 °C and the specified gas concentration. To analyze the fluorescence response of the CHO cells, images were acquired using a laser scanning confocal microscope (Zeiss LSM 710) with a 20 × 0.8 NA objective. The fluorescence intensity of each cell was measured using ImageJ ROI manager.[51–53]

I. Microscopy, image processing, and statistical analysis of redox experiments

Just prior to redox imaging, cells were washed twice and the medium was replaced with Dulbecco's phosphate-buffered saline supplemented with 5% FBS and 10 mmol/l glucose to avoid changes in redox poise resulting from media oxidation.[54] Redox experiments were performed using a 63× oil objective on an inverted fluorescent microscope (Axiovert 200 M, Carl Zeiss, Feldbach, Switzerland) with an environmental control chamber (37 °C and 5% CO_2). Time-resolved images (512 × 512 pixels) were taken with excitation filters 395/11 and 494/20 nm, a 510 nm dichroic mirror, and a 527/20 nm emission filter (Semrock, Rochester, NY). Images were acquired every 45 s for 2 h to monitor the redox status. Following each experiment, the live cell biosensor was calibrated by sequential addition of the strong oxidant diamide and strong reductant DTT while acquiring images every 20 s. Images were exported to Axiovision data analysis software in which the region of interest (containing at least 5 cells) and background intensities were identified. Percent oxidation of Grx1-roGFP2 was calculated from background-corrected fluorescence intensities of both excitation channels in accordance with Eq. (2), where F, F_{ox}, and F_{red} are the 395:494 nm excitation ratios at the steady state, full oxidation, and full reduction, respectively. The fully oxidized and reduced fluorescence intensities at 494 nm are I_{ox} and I_{red}. The analysis of variance was performed to determine the statistical significance between normoxic and hypoxic experimental groups ($p < 0.05$).

$$\left(1 - \left(\frac{R}{1-R} = \frac{F - F_{ox}}{F_{red} - F} * \frac{I_{ox}}{I_{red}}\right)\right) * 100. \tag{2}$$

III. RESULTS AND DISCUSSION

A. Design of open-well microfluidic platform to control oxygen concentrations

A microfluidic platform was designed and fabricated that enables cell studies under controlled oxygen conditions. The device enables easy manipulation of cells, reagents, and media with a micropipette while controlling the amount of dissolved oxygen. The platform is comprised of two PDMS layers, a gas layer, and a cell layer (Fig. 1). The open-well cell layer, residing on top of the gas layer, enables cells to be added into a 4-mm wide cell chamber via a micropipette. After addition of the cell/hydrogel mixture and brief 37 °C incubation for hydrogel encapsulation, culture media can be added directly to the cell chamber via a micropipette. The gas layer runs at the base of the platform and is comprised of 50 parallel channels. Each channel is 20 μm tall, 50 μm wide, and patterned 50 μm apart. Gas streams flow through the channels and diffuse through the PDMS membrane to the cell chamber, enabling control over the amount of dissolved oxygen. Similarly, designed platforms have been proven to enable control over the amount of dissolved oxygen, manipulation of cells, and studies of complex cellular response to hypoxia.[39] Going forward, this work enables understanding of how different design

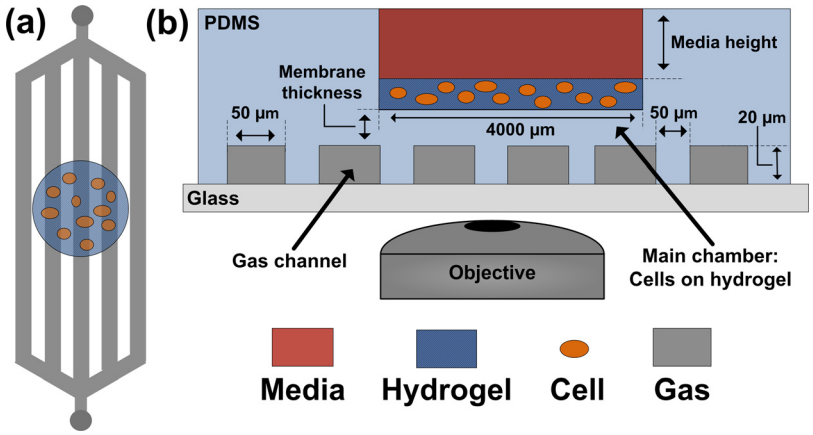

FIG. 1. Schematic of the open-well microfluidic platform. (a) Top down view of the microfluidic platform's gas channels (grey) and cell chamber (blue). (b) Cross sectional view of the microfluidic platform. Cells are introduced into the cell chamber along with media and reagents.

considerations impact the oxygen concentration within the microfluidic platform and demonstrate its utility by performing complex cellular assays.

B. Validation of the dissolved oxygen concentration within the microfluidic platform

To determine the amount of dissolved oxygen within the microfluidic platform, both computational simulations and experimental measurements were performed. For both, a PDMS membrane thickness of 20 μm and a media height of 1.5 mm were used unless stated otherwise. The amount of dissolved oxygen within the microfluidic platform was computationally simulated by developing a model of the device using the finite element analysis software Comsol (Fig. 2). The transient simulation determined the amount of dissolved oxygen at different time points after a gas stream with a composition of 0% oxygen (v/v) was introduced into the microfluidic platform. The simulated amount of dissolved oxygen equilibrated within 5 min of the gas stream introduction. This model was further employed to investigate the effects of the media height, membrane thickness, and the addition of an impermeable barrier on the amount of dissolved oxygen within the platform.

The amount of dissolved oxygen within the microfluidic platform was experimentally measured by analyzing the change in fluorescence of RTDP, the fluorescence of which is quenched in the presence of oxygen. Thus, changes in fluorescence intensity can be correlated with the amount of dissolved oxygen in the system. However, using this method to resolve small differences in the oxygen concentration in a statistically significant manner is challenging due to noise in emission strength and detector capability. Still, the amount of dissolved oxygen within the platform was measured as gas streams with compositions of 0%, 1%, and 5% O_2 (v/v) being introduced (Fig. 3). Expectedly, the amount of dissolved oxygen within the platform changed as the concentration of oxygen in the gas stream was modulated. Furthermore, the amount of dissolved oxygen equilibrated within 10 min of gas being introduced. Overall, the computational simulations predict an amount of dissolved oxygen similar to the experimentally measured values, demonstrating agreement between our computational and experimental results.

C. Effects of an oxygen impermeable barrier on dissolved oxygen concentrations

The open-well design of the microfluidic platform enables easy manipulation of cells and reagents. However, this feature also allows some oxygen from atmospheric air to diffuse to cells residing at the bottom of the cell chamber (Fig. 1). This atmospheric oxygen compromises the control of the amount of dissolved oxygen present in the cellular microenvironment. One method to increase control over the oxygen conditions is to simply place an oxygen impermeable barrier on top of the open-well cell chamber. To determine the effects of placing this

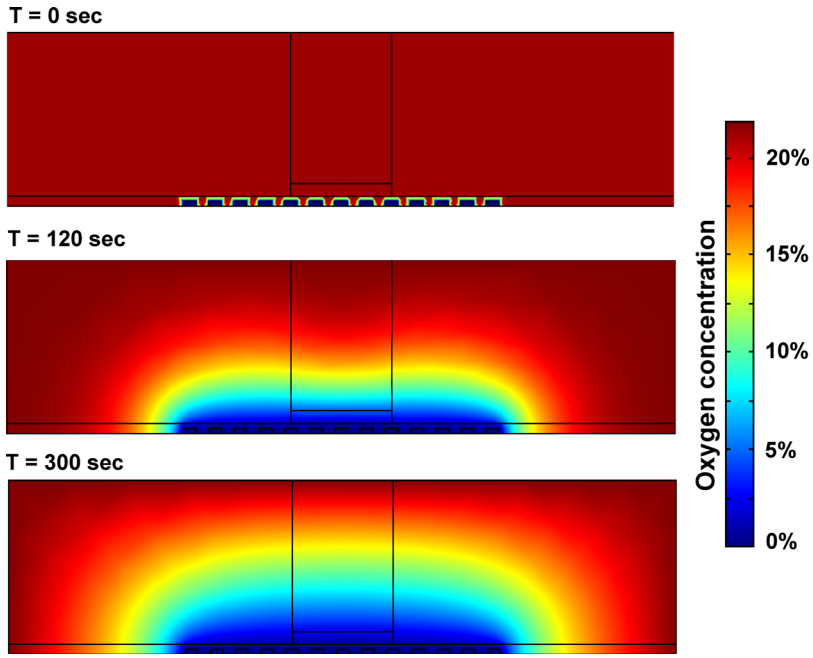

FIG. 2. Computational model developed to simulate the amount of dissolved oxygen within the microfluidic platform. The dissolved oxygen was simulated at different time points after introducing a gas stream with a composition of 0% oxygen (v/v) into the gas channels of the microfluidic platform.

barrier on the microfluidic platform, the equilibrated amount of dissolved oxygen was both simulated and experimentally measured with the open well simply covered by a glass coverslip, which acts as an oxygen impermeable barrier (Fig. 4). The equilibrated amount of dissolved oxygen within the microfluidic platform was reduced from approximately 0.6 mg/l O_2 in the open-well condition to approximately 0.3 mg/l O_2 with the impermeable barrier. The difference in dissolved oxygen within the device with addition of a gas-impermeable barrier was not found to be statistically significant in this study. However, the use of a gas-impermeable coverslip is a

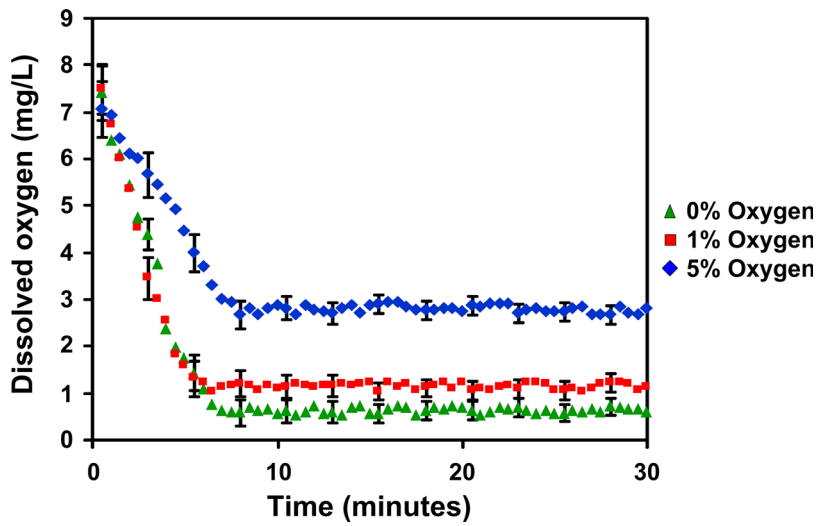

FIG. 3. Experimental measurements of dissolved oxygen in the main chamber of the microfluidic platform. The gas stream composition was varied from 0% to 5% oxygen (v/v). A membrane thickness of 20 μm and a media height of 1.5 mm were used during all measurements. Error bars represent the standard deviation calculated from all experiments for each gas composition; experiments were repeated six times.

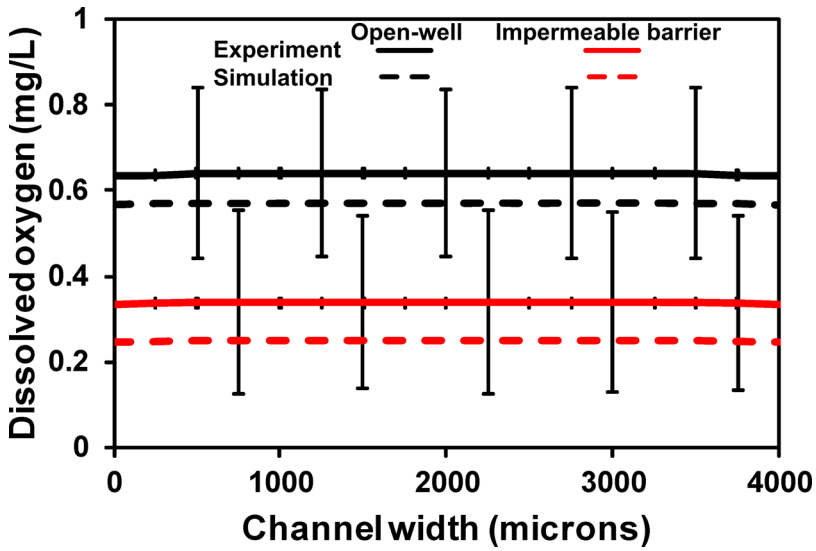

FIG. 4. Dissolved oxygen after equilibration with the top of the microfluidic platform open or covered. The cell chamber was either open to the atmosphere (open-well) or covered by a glass coverslip (impermeable barrier). A membrane thickness of 20 μm, a media height of 1.5 mm, and a gas stream with 0% oxygen (v/v) were used for all measurements. Error bars represent the standard deviation calculated from all experiments for each gas composition; experiments were repeated six times.

simple, mechanistically intuitive method to reduce diffusion of atmospheric oxygen into the microfluidic platform. The trend of decreased oxygen concentrations with a gas-impermeable coverslip displayed in Fig. 4 agrees with this mechanism. Thus, this design consideration provides a potential solution to further reduce oxygen concentrations. Furthermore, by placing but not bonding the coverslip barrier, the platform retains all of the desired functionality, while control over oxygen conditions is increased.

D. Effects of the media height and membrane thickness on dissolved oxygen concentrations

In the designed microfluidic platform, gas diffuses from the gas channel through the PDMS membrane to the cell chamber (Fig. 1). Diffusion of oxygen via this route enables control over the amount of dissolved oxygen within the microfluidic platform. Thus, modulating the PDMS membrane thickness will affect the amount of dissolved oxygen within the solution. To determine the effect of PDMS membrane thickness on the amount of dissolved oxygen, the equilibrated amount of dissolved oxygen was both computationally simulated and experimentally measured [Fig. 5(a)]. The membrane thickness was varied from 20 to 150 μm, resulting in a change in the amount of dissolved oxygen from approximately 0.7 mg/l O_2 to 2.0 mg/l O_2. Expectedly, the amount of dissolved oxygen within the platform increases as the membrane thickness increases. Thus, to reduce the amount of dissolved oxygen, the membrane should be as thin as possible.

Another design parameter for the microfluidic platform that affects the amount of dissolved oxygen is the media height. Oxygen from the atmospheric air diffuses through the media to the cells located at the bottom of the cell chamber. Thus, the relationship between the media height and the amount of dissolved oxygen within the platform was explored. The media height was varied from 0.5 to 1.5 mm, and the amount of dissolved oxygen within the microfluidic platform was experimentally measured and computationally simulated [Fig. 5(b)]. The amount of dissolved oxygen decreased as the media height increased, an effect likely because the increased distance oxygen from the atmospheric air must diffuse to reach the bottom of the cell chamber. In addition, one should note that the media height will change over long time periods due to evaporation, potentially affecting the amount of dissolved oxygen. Overall, both the media height and membrane thickness affect the amount of dissolved oxygen within an open-well microfluidic platform.

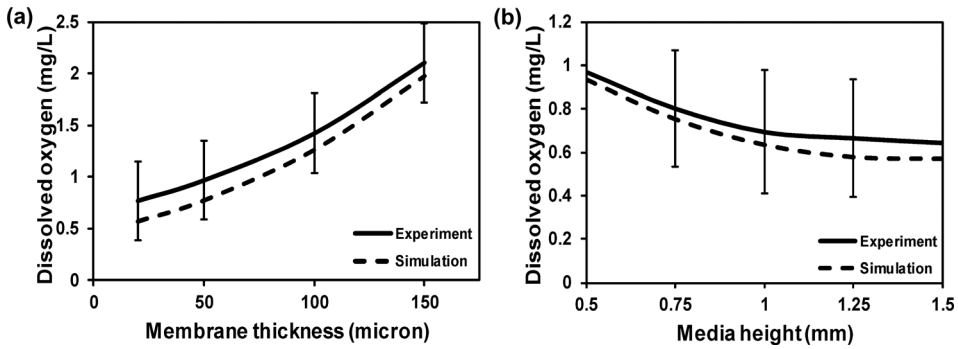

FIG. 5. Dissolved oxygen within the microfluidic platform after equilibration with varying (a) membrane thicknesses and (b) media heights. (a) The membrane thickness was varied from 20 to 150 μm. (b) Media height varied from 0.5 to 1.5 mm. A gas stream with 0% oxygen (v/v) was introduced into the platform for all measurements. Error bars represent the standard deviation calculated from all experiments for each gas composition; experiments were repeated six times.

E. Measuring HIF-α stabilization and transcriptional activity under varying amounts of dissolved oxygen

Sub-physiologic oxygen levels are well known to fundamentally regulate many aspects of cell biology. Many of the cellular effects of hypoxia involve the transcription factor HIF. Thus, measuring HIF levels at varying amounts of dissolved oxygen will help to better understand the link between hypoxia and cell behavior. To measure this and to provide cell context specific validation of the hypoxia platform, a genetically encoded reporter construct consisting of tandem repeats of HIF binding sites in the promoter of the eYFP gene was employed to monitor HIF-α stabilization as a function of hypoxia. The 6 U-HBR (HIF-binding repeats) reporter has previously been demonstrated to correlate with HIF protein levels.[45] Chinese hamster ovary (CHO) cells stably expressing the reporter were introduced into the microfluidic platform and exposed to amounts of dissolved oxygen ranging from 0.3 mg/l O_2 to 6.5 mg/l O_2, as previously demonstrated, for 14 h, and HIF protein levels were measured by analyzing the fluorescent expression of eYFP (Fig. 6). The initial media height for all conditions was 150 μm, a level which was preserved throughout the experiment by adding 5–10 μl boluses of media after hours 5 and 10 to minimize evaporation. HIF protein levels were increased after 12 h of incubation in

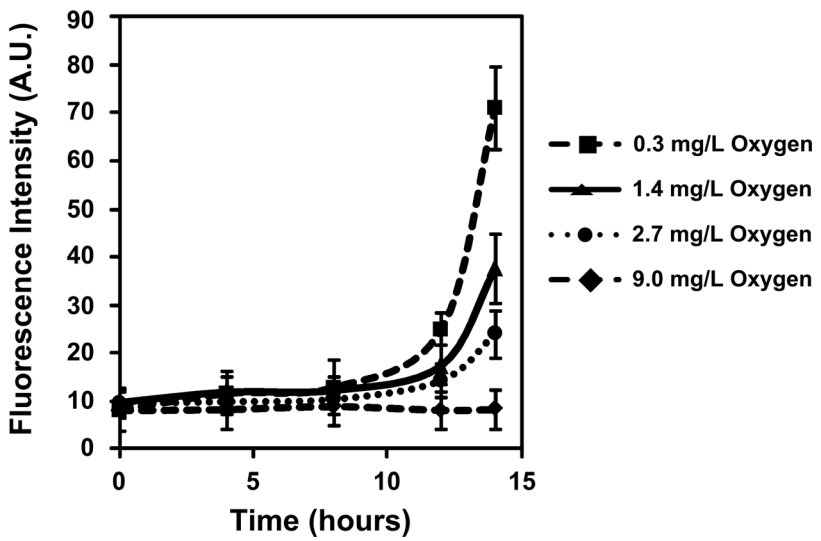

FIG. 6. Stabilization of HIF-α in CHO cells measured using the 6 U-HBR reporter. Measurements were taken from 0 to 14 h. Cells were incubated under varying amounts of dissolved oxygen. Error bars represent the standard deviation calculated from all experiments; experiments were repeated six times resulting in at least 50 cells analyzed for each value.

0.3 mg/l O_2 ($p < 0.0001$) when compared to the initial time point. Furthermore, HIF protein levels in CHO cells incubated for 14 h in 0.3 mg/l O_2 were significantly higher than those at 6.5 mg/l O_2 ($p < 0.0001$). These data demonstrate a clear link between hypoxic cell culture within the open-well microfluidic platform and relevant cellular functional outcomes.

F. Measuring the mitochondrial matrix redox response to hypoxia

Redox reactions dictate the protein shape, modulate enzyme activity, initiate gene transcription, and define cellular metabolism. When redox poise fails and cells become oxidized, cellular death soon follows.[55] Glutathione, which exists in a dynamic redox couple comprised of both an oxidized and a reduced form, is the most abundant non-protein thiol antioxidant in eukaryotic cells, and thus, it is used an indicator of the local redox environment and relative oxidative stress.[56] During hypoxia, glutathione in the cytosol and mitochondrial intermembrane space becomes oxidized, whereas the mitochondrial matrix pool becomes reduced.[15–18,20–24,57] This is both mechanistically intriguing and of potential importance to mitochondrial energy generation. To our knowledge, the redox response of the mitochondrial matrix of transformed cells in hypoxic conditions has not previously been investigated. Thus, A549 lung carcinoma cells expressing mitochondrial matrix targeted Grx1-roGFP2, a redox-sensitive fluorescent biosensor fused to glutaredoxin to improve probe kinetics, were cultured within the open-well platform and exposed to hypoxia (Fig. 7). The Grx1-roGFP2 biosensor has two fluorescent excitation peaks, 395 and 494 nm; the ratio of the fluorescence emission of these channels at 509 nm corresponds to the oxidation/reduction of the compartmentalized glutathione couple.[58,59] Following each experimental observation, the biosensor is calibrated with the addition of a strong oxidant, diamide, followed by a strong reductant, DTT, to define full oxidation and full reduction and to enable calculations of percent oxidation [Fig. 7(b); Eq. (2)].

Percent oxidation of the mitochondrial matrix did not significantly deviate throughout normoxia but underwent a significant 10% reduction during 0.3 mg/l O_2 hypoxic culture ($p < 0.05$) [Fig. 7(c)]. A similar response was observed in non-transformed CHO cells (data not shown). These results are consistent with previous reports in other cell types although the loss of oxidation observed in the mitochondrial matrix is noticeably slower than that reported previously.[20,22–24,57] The extent to which this may reflect differences in freshly isolated primary cells versus long-established oxy-tolerant cell lines is unknown. Despite the understanding of hypoxia as a pro-oxidative insult, the observation of mitochondrial matrix glutathione reduction during hypoxia reinforces the understanding that interorganellar redox poise is independently maintained and distinctly altered by environmental insults.[15,60] The reductive response of the mitochondrial matrix has previously been hypothesized to reflect the production of ROS away from the mitochondrial matrix outward into the intermembrane space or to be mediated by the buildup of matrix reducing equivalents as a result of slowed oxidative phosphorylation.[20,23,57] Distinguishing between these possibilities and further defining the mechanism of mitochondrial matrix reduction in hypoxia will require further investigation. Because mitochondrial redox balance regulates energy production and apoptosis, future studies in this area may yield novel strategies to promote tumor cell death.

IV. CONCLUSIONS

We report the effect of design considerations on an open-well microfluidic platform for cell studies under controlled oxygen conditions. The open-well design of the device enables easy handling and addition of cells and reagents using a micropipette and provides a single combined space in which to propagate, image, and experimentally modulate cell cultures. To validate the amount of dissolved oxygen within the platform, both experimental measurements and computational simulations were performed. Placing a glass coverslip on top of the device provided an oxygen impermeable barrier that enabled enhanced control of dissolved oxygen concentrations. The effects of design parameters such as membrane thickness and media height on the amount of dissolved oxygen within the device were also explored. Finally, two studies of hallmark cellular responses to hypoxia were conducted in the microfluidic platform: HIF-α stabilization and changes to redox homeostasis resulting from ROS production. Overall, the

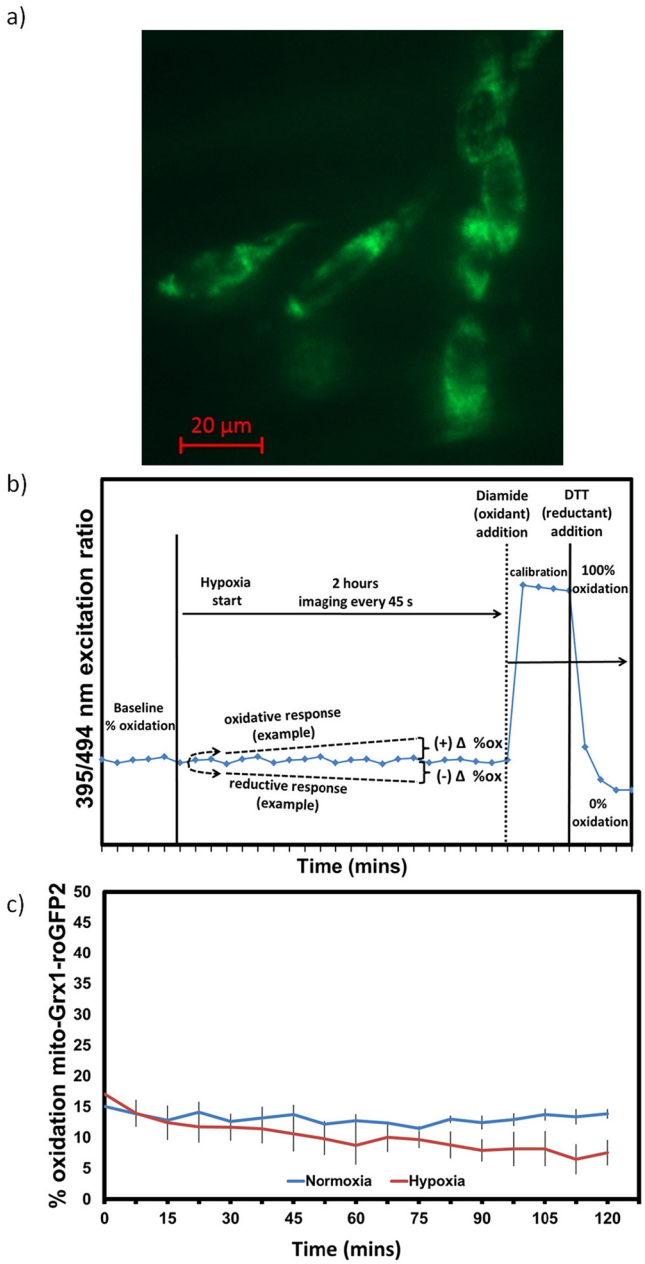

FIG. 7. Measurement of the mitochondrial matrix redox response to hypoxia. (a) Fluorescent image of A549 cells expressing the mito-Grx1-roGFP2 biosensor within the open well microfluidic platform. (b) Schematic of redox experimental workflow. (c) Percent oxidation (mean +/− SEM) of the mito-Grx1-roGFP2 biosensor throughout 2 h of normoxic/hypoxic imaging. Experiments were repeated three times with at least 5 cells analyzed per experiment.

open-well microfluidic platform described provides an ease-of-use approach for studying complex cellular responses to hypoxia.

ACKNOWLEDGMENTS

The support for this study was provided by the Midwest Cancer Nanotechnology Training Center (MTL) and National Institutes of Health grant R33-CA137719 (HRG & PJAK). Dr Shiv Sivaguru is thanked for his assistance with fluorescence microscopy. Jessica Beaudoin is thanked for her assistance with lentiviral transduction.

There are no conflicts to declare.

[1]M. Bache, M. Kappler, H. M. Said, A. Staab, and D. Vordermark, "Detection and specific targeting of hypoxic regions within solid tumors: Current preclinical and clinical strategies," Curr. Med. Chem. **15**(4), 322–338 (2008).
[2]J. M. Brown and W. R. Wilson, "Exploiting tumour hypoxia in cancer treatment," Nat. Rev. Cancer **4**(6), 437–447 (2004).
[3]M. Hockel and P. Vaupel, "Tumor hypoxia: Definitions and current clinical, biologic, and molecular aspects," J. Natl. Cancer Inst. **93**(4), 266–276 (2001).
[4]A. K. Iyer, G. Khaled, J. Fang, and H. Maeda, "Exploiting the enhanced permeability and retention effect for tumor targeting," Drug Discovery Today **11**(17-18), 812–818 (2006).
[5]H. Maeda, J. Wu, T. Sawa, Y. Matsumura, and K. Hori, "Tumor vascular permeability and the EPR effect in macromolecular therapeutics: A review," J. Controlled Release **65**(1-2), 271–284 (2000).
[6]H. Axelson, E. Fredlund, M. Ovenberger, G. Landberg, and S. Pahlman, "Hypoxia-induced dedifferentiation of tumor cells—A mechanism behind heterogeneity and aggressiveness of solid tumors," Seminars Cell Dev. Biol. **16**(4-5), 554–563 (2005).
[7]P. Vaupel and A. Mayer, "Hypoxia in cancer: Significance and impact on clinical outcome," Cancer Metastasis Rev. **26**(2), 225–239 (2007).
[8]W. R. Wilson and M. P. Hay, "Targeting hypoxia in cancer therapy," Nat. Rev. Cancer **11**(6), 393–410 (2011).
[9]S. N. Greer, J. L. Metcalf, Y. Wang, and M. Ohh, "The updated biology of hypoxia-inducible factor," EMBO J. **31**(11), 2448–2460 (2012).
[10]T. Hellwig-Burgel, D. P. Stiehl, A. E. Wagner, E. Metzen, and W. Jelkmann, "Hypoxia-inducible factor-1 (HIF-1): A novel transcription factor in immune reactions," J. Interferon Cytokine Res. **25**(6), 297–310 (2005).
[11]A. Loboda, A. Jozkowicz, and J. Dulak, "HIF-1 and HIF-2 transcription factors - Similar but not identical," Mol. Cells **29**(5), 435–442 (2010).
[12]P. H. Maxwell, "Hypoxia-inducible factor as a physiological regulator," Exp. Physiol. **90**(6), 791–797 (2005).
[13]N. S. Chandel, E. Maltepe, E. Goldwasser, C. E. Mathieu, M. C. Simon, and P. T. Schumacker, "Mitochondrial reactive oxygen species trigger hypoxia-induced transcription," Proc. Natl. Acad. Sci. U.S.A. **95**(20), 11715–11720 (1998).
[14]R. D. Guzy, B. Hoyos, E. Robin, H. Chen, L. P. Liu, K. D. Mansfield *et al.*, "Mitochondrial complex III is required for hypoxia-induced ROS production and cellular oxygen sensing," Cell Metab. **1**(6), 401–408 (2005).
[15]G. B. Waypa, K. A. Smith, and P. T. Schumacker, "O_2 sensing, mitochondria and ROS signaling: The fog is lifting," Mol. Aspects Med. **47–48**, 76–89 (2016).
[16]E. L. Bell, T. A. Klimova, J. Eisenbart, P. T. Schumacker, and N. S. Chandel, "Mitochondrial reactive oxygen species trigger hypoxia-inducible factor-dependent extension of the replicative life span during hypoxia," Mol. Cellular Biol. **27**(16), 5737–5745 (2007).
[17]A. Y. Chi, G. B. Waypa, P. T. Mungai, and P. T. Schumacker, "Prolonged hypoxia increases ROS signaling and RhoA activation in pulmonary artery smooth muscle and endothelial cells," Antioxidants Redox Signaling. **12**(5), 603–610 (2010).
[18]J. R. Desireddi, K. N. Farrow, J. D. Marks, G. B. Waypa, and P. T. Schumacker, "Hypoxia increases ROS signaling and cytosolic Ca^{2+} in pulmonary artery smooth muscle cells of mouse lungs slices," Antioxid. Redox Signaling **12**(5), 595–602 (2010).
[19]P. T. Mungai, G. B. Waypa, A. Jairaman, M. Prakriya, D. Dokic, M. K. Ball *et al.*, "Hypoxia triggers AMPK activation through reactive oxygen species-mediated activation of calcium release-activated calcium channels," Mol. Cellular Biol. **31**(17), 3531–3545 (2011).
[20]S. S. Sabharwal, G. B. Waypa, J. D. Marks, and P. T. Schumacker, "Peroxiredoxin-5 targeted to the mitochondrial intermembrane space attenuates hypoxia-induced reactive oxygen species signaling," Biochem. J. **456**, 337–346 (2013).
[21]G. B. Waypa, R. Guzy, P. T. Mungai, M. M. Mack, J. D. Marks, M. W. Roe *et al.*, "Increases in mitochondrial reactive oxygen species trigger hypoxia-induced calcium responses in pulmonary artery smooth muscle cells," Circ. Res. **99**(9), 970–978 (2006).
[22]G. B. Waypa, J. D. Marks, R. Guzy, P. T. Mungai, J. Schriewer, D. Dokic *et al.*, "Hypoxia triggers subcellular compartmental redox signaling in vascular smooth muscle cells," Circ. Res. **106**(3), 526–535 (2010).
[23]G. B. Waypa, J. D. Marks, R. D. Guzy, P. T. Mungai, J. M. Schriewer, D. Dokic *et al.*, "Superoxide Generated at Mitochondrial Complex III Triggers Acute Responses to Hypoxia in the Pulmonary Circulation," Am. J. Respir. Crit. Care Med. **187**(4), 424–432 (2013).
[24]G. B. Waypa, S. W. Osborne, J. D. Marks, S. K. Berkelhamer, J. Kondapalli, and P. T. Schumacker, "Sirtuin 3 deficiency does not augment hypoxia-induced pulmonary hypertension," Am. J. Respir. Cell Mol. Biol. **49**(6), 885–891 (2013).
[25]M. B. Byrne, M. T. Leslie, H. R. Gaskins, and P. J. A. Kenis, "Methods to study the tumor microenvironment under controlled oxygen conditions," Trends Biotechnol. **32**(11), 556–563 (2014).
[26]H. E. Abaci, R. Devendra, Q. Smith, S. Gerecht, and G. Drazer, "Design and development of microbioreactors for long-term cell culture in controlled oxygen microenvironments," Biomed. Microdevices **14**(1), 145–152 (2012).
[27]K. Funamoto, I. K. Zervantonakis, Y. C. Liu, C. J. Ochs, C. Kim, and R. D. Kamm, "A novel microfluidic platform for high-resolution imaging of a three-dimensional cell culture under a controlled hypoxic environment," Lab Chip **12**(22), 4855–4863 (2012).
[28]G. Mehta, J. Lee, W. Cha, Y. C. Tung, J. J. Linderman, and S. Takayama, "Hard top soft bottom microfluidic devices for cell culture and chemical analysis," Anal. Chem. **81**(10), 3714–3722 (2009).
[29]C. J. Ochs, J. Kasuya, A. Pavesi, and R. D. Kamm, "Oxygen levels in thermoplastic microfluidic devices during cell culture," Lab Chip **14**(3), 459–462 (2014).
[30]M. Skolimowski, M. W. Nielsen, J. Emneus, S. Molin, R. Taboryski, C. Sternberg *et al.*, "Microfluidic dissolved oxygen gradient generator biochip as a useful tool in bacterial biofilm studies," Lab Chip **10**(16), 2162–2169 (2010).
[31]M. Adler, M. Polinkovsky, E. Gutierrez, and A. Groisman, "Generation of oxygen gradients with arbitrary shapes in a microfluidic device," Lab Chip **10**(3), 388–391 (2010).
[32]S. Martewicz, F. Michielin, E. Serena, A. Zambon, M. Mongillo, and N. Elvassore, "Reversible alteration of calcium dynamics in cardiomyocytes during acute hypoxia transient in a microfluidic platform," Integr. Biol. **4**(2), 153–164 (2012).

[33]S. C. Oppegard and D. T. Eddington, "A microfabricated platform for establishing oxygen gradients in 3-D constructs," Biomed. Microdevices **15**(3), 407–414 (2013).
[34]M. Polinkovsky, E. Gutierrez, A. Levchenko, and A. Groisman, "Fine temporal control of the medium gas content and acidity and on-chip generation of series of oxygen concentrations for cell cultures," Lab Chip **9**(8), 1073–1084 (2009).
[35]P. C. Thomas, S. R. Raghavan, and S. P. Forry, "Regulating oxygen levels in a microfluidic device," Anal. Chem. **83**(22), 8821–8824 (2011).
[36]A. P. Vollmer, R. F. Probstein, R. Gilbert, and T. Thorsen, "Development of an integrated microfluidic platform for dynamic oxygen sensing and delivery in a flowing medium," Lab Chip **5**(10), 1059–1066 (2005).
[37]C. B. Allen, B. K. Schneider, and C. W. White, "Limitations to oxygen diffusion and equilibration in in vitro cell exposure systems in hyperoxia and hypoxia," Am. J. Physiol.: Lung Cell. Mol. Physiol. **281**(4), L1021–L10L7 (2001).
[38]M. D. Brennan, M. L. Rexius-Hall, L. J. Elgass, and D. T. Eddington, "Oxygen control with microfluidics," Lab Chip **14**(22), 4305–4318 (2014).
[39]J. F. Lo, E. Sinkala, and D. T. Eddington, "Oxygen gradients for open well cellular cultures via microfluidic substrates," Lab Chip **10**(18), 2394–2401 (2010).
[40]C. C. Peng, W. H. Liao, Y. H. Chen, C. Y. Wu, and Y. C. Tung, "A microfluidic cell culture array with various oxygen tensions," Lab Chip **13**(16), 3239–3245 (2013).
[41]B. H. Jo, L. M. Van Lerberghe, K. M. Motsegood, and D. J. Beebe, "Three-dimensional micro-channel fabrication in polydimethylsiloxane (PDMS) elastomer," J. Microelectromech. Syst. **9**(1), 76–81 (2000).
[42]H. Lorenz, M. Despont, N. Fahrni, N. LaBianca, P. Renaud, and P. Vettiger, "SU-8: a low-cost negative resist for MEMS," J. Micromech. Microeng. **7**(3), 121–124 (1997).
[43]P. Renaud, H. van Lintel, M. Heuschkel, and L. Guerin, in *Photo-Polymer Microchannel Technologies and Applications*, edited by D. J. Harrison and A. VanDenBerg (Springer, 2000), pp. 17–22.
[44]Y. N. Xia and G. M. Whitesides, "Soft lithography," Angew. Chem., Int. Ed. **37**(5), 550–575 (1998).
[45]W. Zhou, T. L. Dosey, T. Biechele, R. T. Moon, M. S. Horwitz, and H. Ruohola-Baker, "Assessment of hypoxia inducible factor levels in cancer cell lines upon hypoxic induction using a novel reporter construct," Plos One **6**(11), e27460 (2011).
[46]G. Mehta, K. Mehta, D. Sud, J. W. Song, T. Bersano-Begey, N. Futai *et al.*, "Quantitative measurement and control of oxygen levels in microfluidic poly(dimethylsiloxane) bioreactors during cell culture," Biomed. Microdevices **9**(2), 123–134 (2007).
[47]W. Zhong, P. Urayama, and M. A. Mycek, "Imaging fluorescence lifetime modulation of a ruthenium-based dye in living cells: The potential for oxygen sensing," J. Phys. D-Appl. Phys. **36**(14), 1689–1695 (2003).
[48]Y.-A. Chen, A. D. King, H.-C. Shih, C.-C. Peng, C.-Y. Wu, W.-H. Liao *et al.*, "Generation of oxygen gradients in microfluidic devices for cell culture using spatially confined chemical reactions," Lab Chip **11**(21), 3626–3633 (2011).
[49]L. Wang, W. Liu, Y. Wang, J-c. Wang, Q. Tu, R. Liu *et al.*, "Construction of oxygen and chemical concentration gradients in a single microfluidic device for studying tumor cell-drug interactions in a dynamic hypoxia microenvironment," Lab Chip **13**(4), 695–705 (2013).
[50]B. Jiang, C. Ren, Y. Li, Y. Lu, W. Li, Y. Wu *et al.*, "Sodium sulfite is a potential hypoxia inducer that mimics hypoxic stress in *Caenorhabditis elegans*," JBIC J. Biol. Inorg. Chem. **16**(2), 267–274 (2011).
[51]M. D. Abràmoff, P. J. Magalhães, and S. J. Ram, Image Processing with Image J **11**, 36–43 (2004).
[52]J. D. Lang, S. M. Berry, G. L. Powers, D. J. Beebe, and E. T. Alarid, "Hormonally responsive breast cancer cells in a microfluidic co-culture model as a sensor of microenvironmental activity," Integr. Biol. **5**(5), 807–816 (2013).
[53]M. B. Byrne, L. Trump, A. V. Desai, L. B. Schook, H. R. Gaskins, and P. J. A. Kenis, "Microfluidic platform for the study of intercellular communication via soluble factor-cell and cell-cell paracrine signaling," Biomicrofluidics **8**(4), 044104 (2014).
[54]V. L. Kolossov, J. N. Beaudoin, W. P. Hanafin, S. J. DiLiberto, P. J. A. Kenis, and H. R. Gaskins, "Transient light-induced intracellular oxidation revealed by redox biosensor," Biochem. Biophys. Res. Commun. **439**(4), 517–521 (2013).
[55]D. Trachootham, W. Lu, M. A. Ogasawara, N. R.-D. Valle, and P. Huang, "Redox regulation of cell survival," Antioxid. Redox Signaling **10**(8), 1343–1374 (2008).
[56]F. Q. Schafer and G. R. Buettner, "Redox environment of the cell as viewed through the redox state of the glutathione disulfide/glutathione couple," Free Radical Biol. Med. **30**(11), 1191–1212 (2001).
[57]B. C. Yin, G. Barrionuevo, and S. G. Weber, "Optimized real-time monitoring of glutathione redox status in single pyramidal neurons in organotypic hippocampal slices during oxygen-glucose deprivation and reperfusion," ACS Chem. Neurosci. **6**(11), 1838–1848 (2015).
[58]C. T. Dooley, T. M. Dore, G. T. Hanson, W. C. Jackson, S. J. Remington, and R. Y. Tsien, "Imaging dynamic redox changes in mammalian cells with green fluorescent protein indicators," J. Biol. Chem. **279**(21), 22284–22293 (2004).
[59]A. J. Meyer and T. P. Dick, "Fluorescent Protein-Based Redox Probes," Antioxid. Redox Signaling **13**(5), 621–650 (2010).
[60]M. S. Attene-Ramos, K. Kitiphongspattana, K. Ishii-Schrade, and H. R. Gaskins, "Temporal changes of multiple redox couples from proliferation to growth arrest in IEC-6 intestinal epithelial cells," Am. J. Physiol.: Cell Physiol. **289**(5), C1220–C12C8 (2005).